OMTN, Volume *21*

Supplemental Information

MicroRNA-19a-PTEN Axis Is Involved in the Developmental Decline of Axon Regenerative Capacity in Retinal Ganglion Cells

Heather K. Mak, Jasmine S.Y. Yung, Robert N. Weinreb, Shuk Han Ng, Xu Cao, Tracy Y.C. Ho, Tsz Kin Ng, Wai Kit Chu, Wing Ho Yung, Kwong Wai Choy, Chi Chiu Wang, Tin Lap Lee, and Christopher Kai-shun Leung

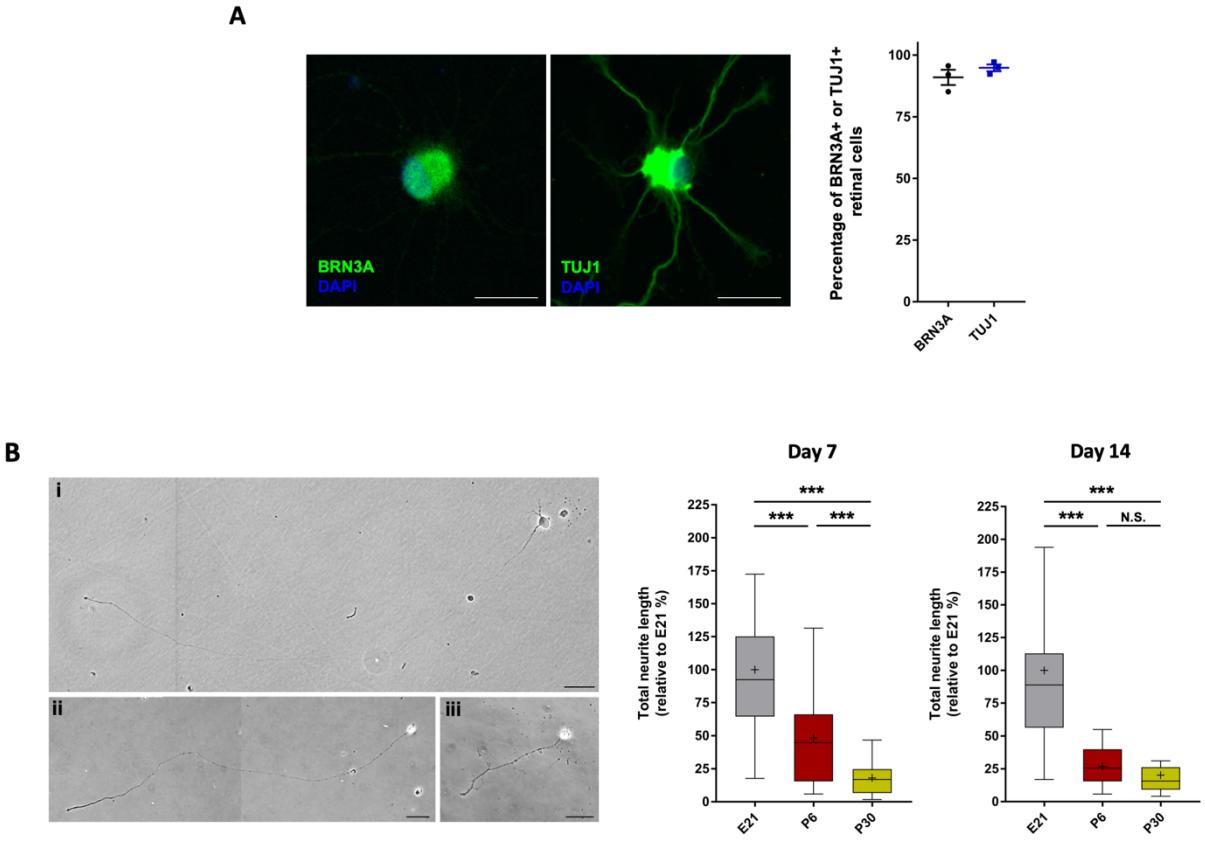

Figure S1. Developmental Decline of Axon Regenerative Capacity in Retinal Ganglion Cells.

(A) *(left)* Immunofluorescence images of BRN3A and TUJ1 staining of retinal ganglion cells (RGCs) isolated from Sprague Dawley (SD) rats using CD90.1 antibodies tagged with magnetic microbeads (Miltenyi Biotec). Scale: 25 µm. *(right)* Purity of RGC isolation was estimated from single-cell analysis of the proportion of BRN3A-positive or TUJ1-positive retinal cells (n=398 total retinal cells from 3 experimental replicates were counted). **(B)** *(left)* Bright field images of RGCs purified from (i) embryonic day 21 (E21), (ii) post-natal day 6 (P6), and (iii) post-natal day 30 (P30) SD rats. Scale bar: 50 µm. *(right)* The total neurite lengths were measured on day 7 and 14 *in vitro*. Single-cell analysis showed that P6 and P30 RGC neurite lengths were significantly shorter than those of E21 RGCs (Day 7: E21 vs. P6, $p<0.0001$; E21 vs. P30, $p<0.0001$; P6 vs. P30, $p<0.0001$; Day 14: E21 vs. P6, $p<0.0001$; E21 vs. P30, $p<0.0001$; P6 vs. P30, $p=0.129$; n=63 E21 RGCs, n=72 P6 RGCs, and n=84 P30 RGCs; n=2 experimental replicates). Unpaired two-tailed Student's t-test was used for all comparisons; ***$p<0.001$; N.S.=not significant. All boxes show the 25th, 50th (median), and 75th percentiles; + represents the data mean; whiskers follow a Turkey boxplot distribution (without outliers) and represent the lower and upper ranges of the data within 1.5x the interquartile range (IQR). All values are in mean ± SEM.

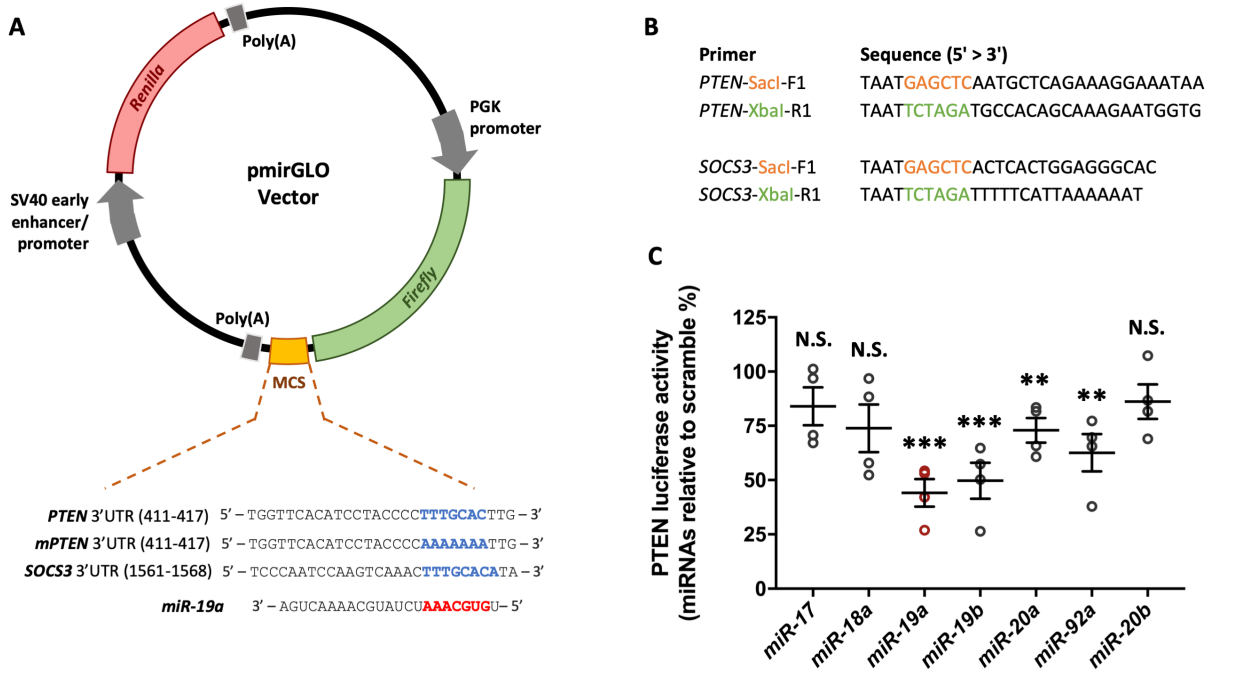

Figure S2. Construct Designs of Dual Luciferase Plasmids to Examine the Binding of miR-19a onto *PTEN*, *mPTEN*, and *SOCS3* 3'UTR in Retinal Ganglion Cells.

(A) The construct design of pmirGLO dual luciferase plasmid. Perfect complementarity of the miR-19a seed sequence *(red boldface)* onto miR-19a binding sites *(blue)* on *PTEN* and *SOCS3* 3'UTR would suppress translation of the *Firefly* luciferase transcript, which decreases *Firefly* luciferase activity, reducing emitted bioluminescent signals upon luciferin oxygenation. *mPTEN* 3'UTR sequence mutated miR-19a binding sites. All *Firefly* luciferase signals were normalized to *Renilla* luciferase signals that are unaffected by miR-19a binding as an endogenous control. MCS, multiple cloning site. **(B)** The primer sequences for cloning of *PTEN* and *SOCS3* 3'UTR into dual luciferase plasmids. **(C)** Dual luciferase assays of *PTEN* 3'UTR after transfection with miR-17, miR-18a, miR-19a, miR-19b, miR-20a, miR-92a, or miR-20b mimic oligos, compared with scramble oligos in P6 RGCs. There was a suppression of the PTEN luciferase by miR-19a, miR-19b, miR-20a, and miR-92a, respectively (miR-19a, $p=0.0001$; miR-19b, $p=0.001$; miR-20a, $p=0.003$; miR-92a, $p=0.005$; $n=4$ experimental replicates per group). miR-17 miR-18a, and miR-20b did not significantly suppress PTEN luciferase activity ($p\geq0.055$). All *Firefly* luciferase was normalized to *Renilla* activity. All values are in mean ± SEM. Unpaired two-tailed Student's t-test was used for all comparisons; **$p<0.01$, ***$p<0.001$, N.S.=not significant.

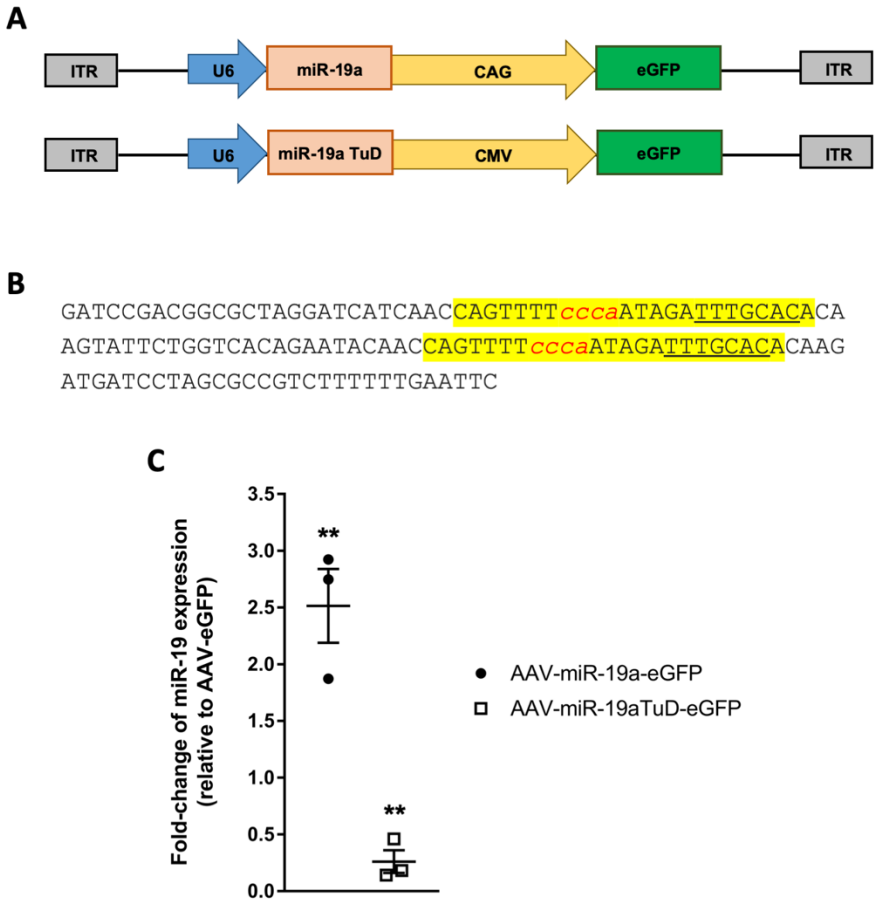

Figure S3. Construct Designs of Adeno-associated Virus (AAV) Plasmids for Delivery of miR-19a and miR-19a Tough Decoy (TuD) to Retinal Ganglion Cells.

(A) Schematic representation of the miR-19a- and miR-19aTuD-expressing AAV vectors. CAG, hybrid construct consisting the cytomegalovirus (CMV) enhancer fused to the chicken β-actin promoter, CMV, cytomegalovirus promoter, eGFP, enhanced green fluorescent protein, ITR, inverted terminal repeats, U6, U6 promoter. **(B)** Sequence of the miR-19a TuD construct. The miR-19a binding site is highlighted in yellow with miRNA seed sequence underlined. An RNA bulge for imperfect miRNA complementarity to enhance miRNA binding efficiency was induced using *ccca* inserts *(red italicized text)*. **(C)** miR-19a levels increased by 2.5±0.3-fold in RGCs transduced with AAV-miR-19a-eGFP, and decreased by 74±9.9% in RGCs transduced with AAV-miR-19aTuD-eGFP using TaqMan qRT-PCR (AAV-miR-19a-eGFP, p=0.010; AAV-miR-19aTuD-eGFP, p=0.002; n=3 experimental replicates per group). Expression values were normalized to AAV-eGFP-transduced P6 RGCs. All values are in mean ± SEM. Unpaired two-tailed Student's t-test was used for all comparisons; **p<0.01.

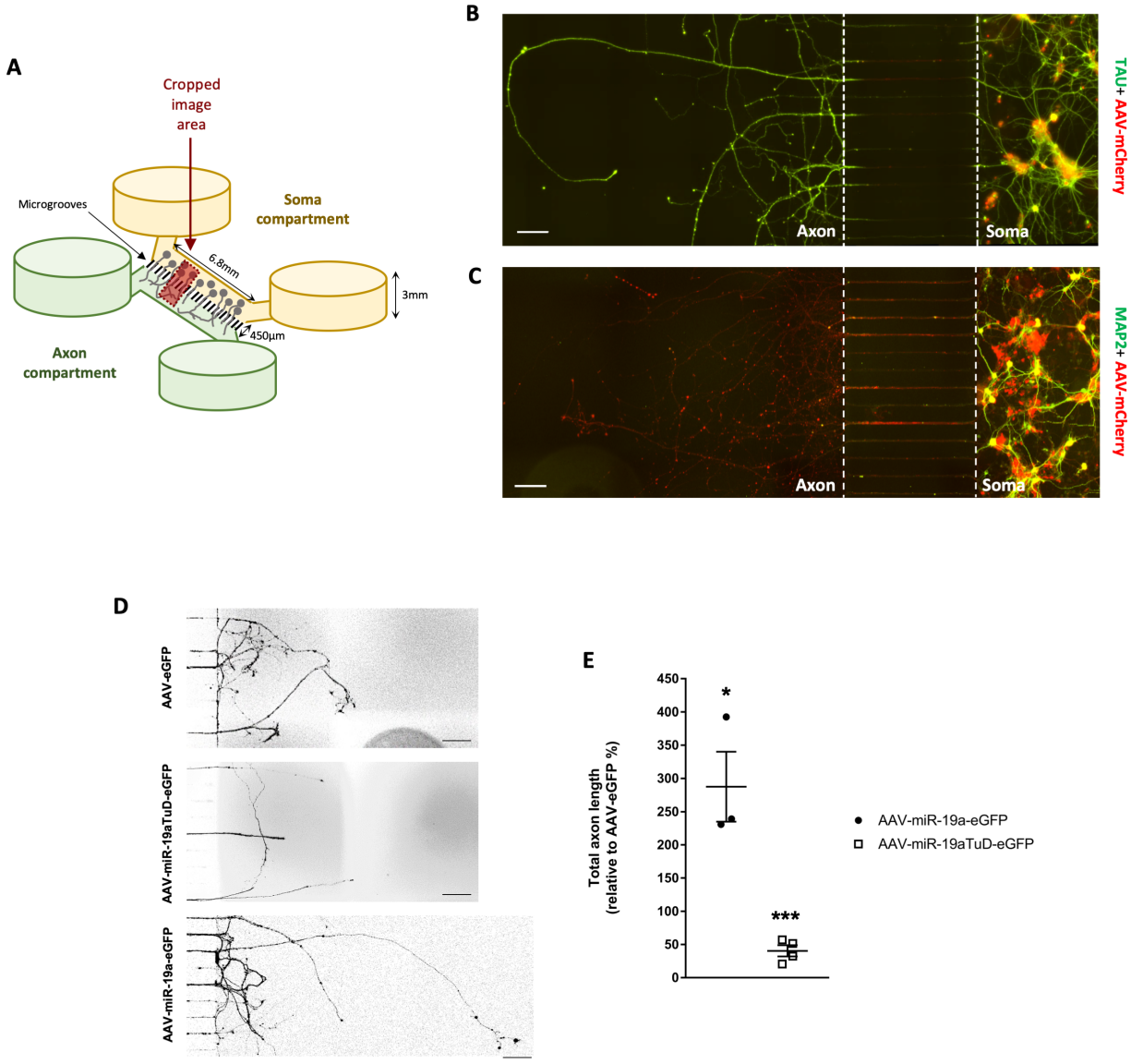

Figure S4. Immunofluorescence Staining of TAU and MAP2 in Retinal Ganglion Cells Cultured in Microfluidic Chambers and the Impact of Overexpression and Inhibition of miR-19a on Axon Extension.

(A) A figure illustration of the design and features of the microfluidic chamber. Cropped image areas of axon-specific TAU **(B)** and dendrite-specific MAP2 **(C)** immunofluorescence staining in P6 RGCs using a microfluidic chamber with indented microgrooves separating the axon from the soma. TAU is detected in both the soma and axon compartments *(left)*, whereas MAP2 remains only in the soma compartment *(right)*, confirming that only axons extend into the axon compartment of microfluidic chambers. AAV-mCherry was used to visualize the RGCs. Scale bar: 100 µm. **(D)** Fluorescence microscopy images of AAV-miR-19aTuD-eGFP- and AAV-miR-19a-eGFP-transduced P6 RGCs in cropped image areas of microfluidic chambers at day-in-vitro 14. Scale bar: 100 µm. **(E)** Comparisons of total axon length between AAV-miR-19aTuD-eGFP- (n=4 experimental replicates) or AAV-miR-19a-eGFP-transduced (n=3 experimental replicates) RGCs and AAV-eGFP-transduced RGCs (n=7 experimental replicates) on day 14 *in vitro*. Compared with AAV-eGFP-transduced P6 RGCs, axon lengths were significantly shorter in AAV-miR-19aTuD-eGFP-tranduced P6 RGCs and significantly longer in AAV-miR-19a-eGFP-transduced P6 RGCs (AAV-miR-19a-eGFP, $p=0.034$; AAV-miR-19aTuD-eGFP, $p=0.0004$). All values are in mean ± SEM. Unpaired two-tailed Student's t-test was used for all comparisons; *$p<0.05$; ***$p<0.001$.

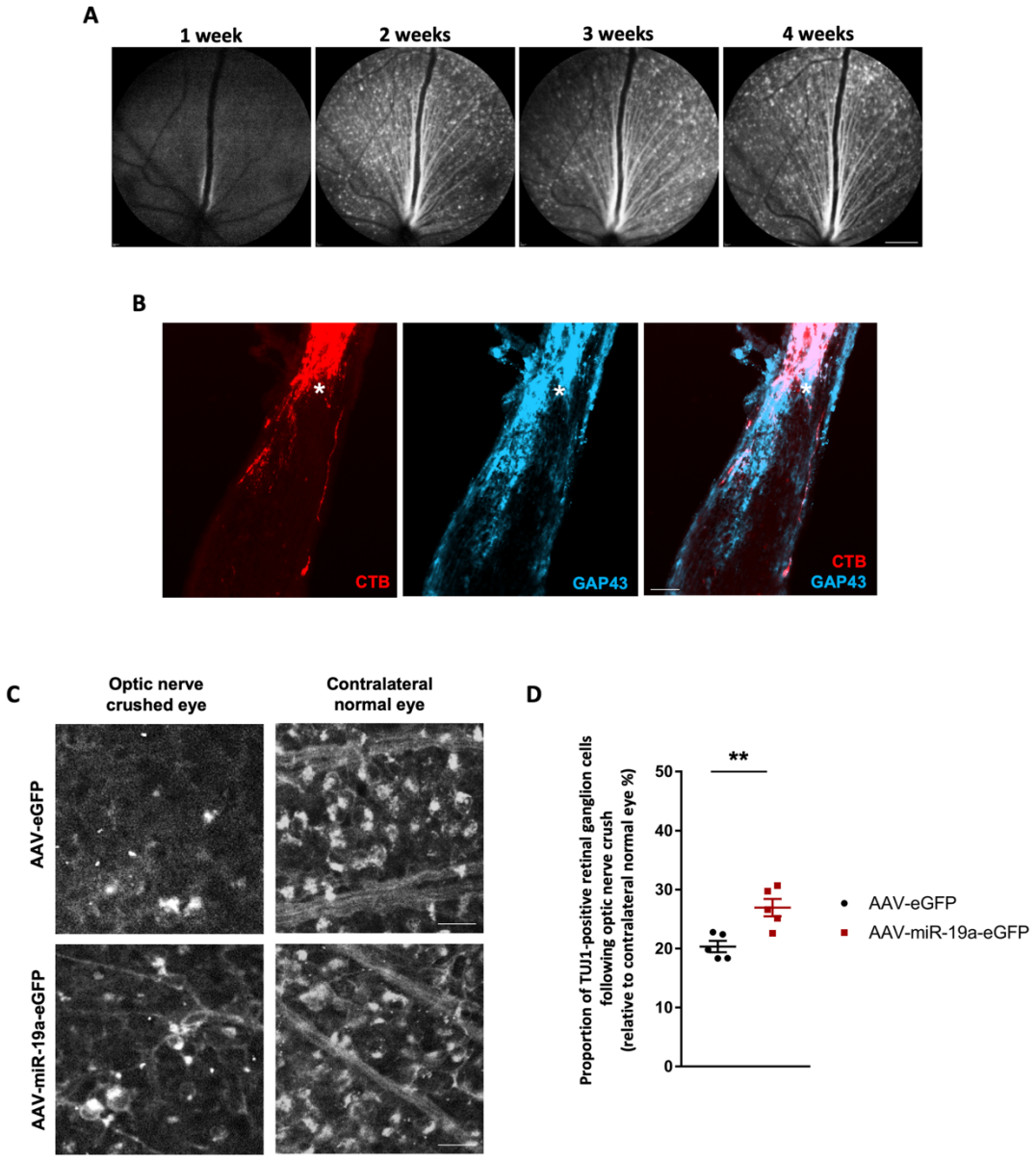

Figure S5. Time-lapse *In Vivo* Retinal Imaging After Intravitreal Injection of AAV-miR-19a-EGFP, Immunofluorescent Staining of GAP43 in the Optic Nerve, and Retinal Ganglion Cell Survival After Optic Nerve Crush.

(A) Confocal scanning laser ophthalmoscopy images of the retina of a C57BL/6J mouse at 1 week, 2 weeks, 3 weeks, and 4 weeks after intravitreal injection of AAV-miR-19a-eGFP. AAV transduction peaked at 2-3 weeks after the intravitreal injection. Scale bar: 200 µm. **(B)** Images of GAP43 *(blue)* immunofluorescence staining and CTB *(red)* in the optic nerve from an eye intravitreally injected with AAV-miR-19a-eGFP at 4 weeks following optic nerve crush. White asterisk indicates optic nerve crush site. Scale bar: 50 µm. **(C)** Images of immunofluorescence staining of TUJ1 in retinal whole-mounts after transduction with AAV-eGFP *(top)* or AAV-miR-19a-eGFP *(bottom)* at 4 weeks following optic nerve crush. Scale bar: 25 µm. **(D)** Proportion of TUJ1-positive retinal ganglion cells following optic nerve crush relative to contralateral normal eye ($p=0.006$; $n=5$ mice for each group). All values are in mean ± SEM. Unpaired two-tailed Student's t-test was used for all comparisons; $^{**}p<0.01$.

Table S1. Microarray Analysis of Differentially Expressed MicroRNA in Retinal Ganglion Cells Purified from Embryonic Day 21 (E21) and Post-natal Day 30 (P30) Sprague Dawley Rats. Only microRNAs with ≥4-fold difference in the expression levels between E21 and P30 RGCs with Benjamini-Hochberg corrected $p<0.05$ are listed.

	E21 vs. P30		
miRNA	**Regulation**	**Fold Change**	**p**
rno-miR-17-5p	down	3742.68	1.67E-04
rno-miR-20b-5p	down	3549.30	1.67E-04
rno-miR-19a	down	2550.93	1.67E-04
rno-miR-18a	down	1771.39	1.67E-04
rno-miR-206	up	1522.66	7.09E-04
rno-miR-20a	down	1288.00	2.47E-02
rno-miR-216a	down	1222.42	2.57E-04
rno-miR-217	down	948.58	2.57E-04
rno-miR-216b-5p	down	739.71	2.57E-04
rno-miR-29c*	up	663.96	1.03E-03
rno-miR-301b	down	558.14	2.63E-04
rno-miR-330*	up	490.72	1.14E-03
rno-miR-370	down	452.93	3.69E-04
rno-miR-130b	down	422.48	4.46E-02
rno-miR-219-5p	down	360.41	4.27E-03
rno-miR-532-5p	down	339.67	2.63E-04
rno-miR-412*	up	255.90	1.73E-03
rno-miR-34b	down	239.96	2.54E-03
rno-miR-484	down	232.25	2.98E-04
rno-miR-34c	down	228.62	8.71E-04
rno-miR-322	down	222.98	5.74E-04
rno-miR-29a	up	214.24	2.98E-04
rno-miR-362*	down	209.71	6.69E-04
rno-miR-375	up	183.77	2.34E-03
rno-miR-31*	up	172.39	2.34E-03
rno-miR-363	down	158.35	3.69E-04
rno-miR-33	down	154.96	5.90E-03
rno-miR-488	down	150.82	1.03E-03
rno-miR-532-3p	down	146.02	7.19E-04
rno-miR-3559-5p	down	124.47	1.03E-03
rno-miR-134	down	114.61	9.26E-03
rno-miR-298	down	89.88	2.49E-03
rno-miR-3593-3p	down	86.47	3.17E-02
rno-miR-181c*	down	85.74	6.30E-04
rno-miR-374	down	84.62	6.69E-04
rno-miR-350	down	81.70	5.74E-04

rno-miR-129-2*	up	78.97	5.74E-04
rno-miR-325-5p	down	77.82	1.03E-03
rno-miR-423*	down	73.93	4.48E-03
rno-miR-129-1*	up	65.63	1.14E-03
rno-miR-211	up	60.19	1.84E-02
rno-miR-130b*	down	53.86	1.18E-03
rno-miR-20a*	down	49.36	8.71E-04
rno-miR-129	up	30.57	2.49E-03
rno-miR-99b*	down	29.13	2.49E-03
rno-miR-19b	down	27.80	1.59E-03
rno-miR-31	up	17.40	4.67E-03
rno-miR-92a	down	15.90	3.16E-03
rno-miR-106b	down	14.27	3.40E-03
rno-let-7b	up	14.14	2.83E-03
rno-miR-485	up	12.32	4.67E-03
rno-miR-29c	up	11.46	3.91E-03
rno-miR-93	down	10.78	5.09E-03
rno-miR-132	up	10.32	8.98E-03
rno-let-7c	up	9.26	5.09E-03
rno-miR-383	up	9.26	9.35E-03
rno-let-7d	up	7.32	8.21E-03
rno-miR-130a	down	7.25	1.13E-02
rno-miR-664	up	7.03	2.79E-02
rno-miR-301a	down	6.55	3.07E-02
rno-miR-127	up	6.47	1.26E-02
rno-miR-183	up	6.38	1.84E-02
rno-miR-328a	up	6.26	1.60E-02
rno-miR-128	up	6.25	1.39E-02
rno-miR-7a	up	5.94	3.49E-02
rno-miR-431	down	5.60	1.71E-02
rno-miR-539	up	5.47	4.92E-02
rno-miR-15b	down	5.28	2.02E-02
rno-miR-146b	up	5.17	3.63E-02
rno-miR-25	down	4.86	1.77E-02
rno-miR-376b-5p	up	4.59	2.85E-02
rno-miR-329	up	4.58	3.63E-02
rno-let-7f	up	4.56	2.85E-02
rno-miR-23b	up	4.53	2.53E-02
rno-miR-341	down	4.46	2.79E-02
rno-let-7a	up	4.19	2.85E-02

Table S3. List of Primary and Secondary Antibodies for Immunocytochemistry (ICC) and Western Blot (WB).

Antibody	Source (Catalog Number)	Working Concentration
Primary antibodies		
Mouse monoclonal anti-beta-Actin clone AC-15	Sigma (A3854)	WB 1:10,000
Rabbit monoclonal anti-BRN3A	Abcam (ab81213)	ICC 1:50
Rabbit polyclonal anti-GAP43	Abcam (ab12274)	ICC 1:200
Mouse monoclonal anti-GAPDH	Thermo Fisher (AM4300)	WB 1:10,000
Mouse monoclonal anti-MAP2	Upstate (05-346)	ICC 1:200
Rabbit monoclonal anti-PTEN	Cell Signaling (9559)	ICC 1:100, WB 1:500
Mouse monoclonal anti-SOCS3	Abcam (ab14939)	WB 1:500
Rabbit monoclonal anti-TAU	Abcam (ab32057)	ICC 1:200
Mouse monoclonal anti-TUJ1	Millipore (MAB5564)	ICC 1:200
Rabbit polyclonal anti-TUJ1	Covance (PRB-425P)	ICC 1:500
Secondary antibodies		
Goat anti-rabbit Alexa Fluor® 350	Invitrogen (A-21068)	ICC 1:1000
Goat anti-mouse Alexa Fluor® 488	Invitrogen (A-11001)	ICC 1:1000
Goat anti-rabbit Alexa Fluor® 488	Invitrogen (A-11008)	ICC 1:1000
Goat anti-mouse Rhodamine Red	Invitrogen (R-6393)	ICC 1:1000
Goat anti-rabbit Rhodamine Red	Invitrogen (R-6394)	ICC 1:1000

Table S2. A Cluster of 314 Downstream Targets of the miR-17-92 Family with Significant Association with Neuron Projection Development Using the PANTHER Classification System.

Video S1. Axon Regeneration of a Retinal Ganglion Cell Transduced with AAV-miR-19a-EGFP After Axotomy.

Video S2. Axon Regeneration of a Retinal Ganglion Cell Transduced with AAV-EGFP After Axotomy.

Data S1. Customized MATLAB program for single-cell analysis of RGC axon length and total neurite length.

Data S2. Customized MATLAB program for microfluidic chamber analysis of total RGC axon length.